International Symposium
On Turbulence and Shear Flow
Phenomena (TSFP-9)
June 30 - July 3, 2015 *Melbourne, Australia*

MINIMAL DYNAMICS OF SELF-SUSTAINING ATTACHED EDDIES IN A TURBULENT CHANNEL

Yacine Bengana
Département de Mécanique,
Université Pierre et Marie Curie (UPMC),
4 Place Jussieu, 75005 Paris, France
Bybengana@gmail.com

Yongyun Hwang
Department of Aeronautics,
Imperial College London,
SW7 2AZ, London, UK.
y.hwang@imperial.ac.uk

ABSTRACT

Very recently, we have performed a numerical experiment designed to simulate only the energy-containing motions at a prescribed spanwise length scale using their self-sustaining nature (Hwang, 2015). The computed statistical structure of each of the energy containing-motions have been found to be self-similar with respect to the spanwise length scale, proportional to the distance from the wall. More importantly, the statistical structure was found to be remarkably similar to that given in the original theory of Townsend, demonstrating the existence of the attached eddies as energy-containing motions contributing to the logarithmic layer. In this work, we extend the previous work to explore the dynamical self-similarity of each of the attached eddies. It is shown that each of the attached eddies exhibit the so-called 'self-sustaining process' composed of 1) streak amplification via the lift-up effect, 2) streak breakdown via the secondary instability, 3) nonlinear regeneration of streamwise vortical structure. This process occurs self-similarly with respect to the spanwise length scale of each of the attached eddies and results in the time scale given by $Tu_\tau/L_z \simeq 2 \sim 3$.

Introduction

Although a non-negligible number of literatures have used the term 'attached eddies' to refer to some fluid motions contributing to the region close the wall, Townsend (1976) originally introduced it to strictly refer to the energy-containing motions, the size of which is proportional to the distance from the wall. Townsend (1976) insightfully deduced such a nature of the energy-containing motions in wall-bounded turbulence from the logarithmic dependence of the mean-velocity profile (i.e. attached eddy hypothesis), thus the term 'attached eddies' basically indicates all the energy-containing motions (i.e. coherent structures) given in a hierarchial form in any kind of wall-bounded turbulent flows showing the logarithmic mean-velocity profile (Perry & Chong, 1982).

Under the assumption that each of the attached eddies is self-similar with respect to its size, Townsend (1976) predicted that the wall-normal profile of turbulence intensities of the wall-parallel velocity components would exhibit a logarithmic dependence, while that of the wall-normal velocity component and the Reynolds stress would be constant in the logarithmic region. During the last decade, there have been a growing body of numerical and experimental evidence which confirms this feature (Jiménez & Hoyas, 2008; Marusic *et al.*, 2013), and it is now very likely that the coherent structures in wall-bounded turbulence are in the form of Townsend's attached eddies.

Very recently, we have performed a numerical experiment, which is designed to simulate only the energy-containing motions at a prescribed spanwise length scale (Hwang, 2015) using their self-sustaining nature (Hwang & Cossu, 2010*b*, 2011). It was shown that the self-sustaining energy-containing motions at a given spanwise length scale is self-similar with respect to the spanwise length scale, and their statistical structure is consistent with that given in the original theory, demonstrating the existence of the attached eddies with directly supporting evidence. The single attached eddy was also found to be composed of a long streak reaching the near-wall region and several quasi-streamwise vortices aligned to that. For a given spanwise length between $\lambda_z^+ \simeq 100$ and $\lambda_z \simeq 1.5h$ in a turbulent channel where h is its half height, the former is found to be self-similar along

$$y \simeq 0.1\lambda_z \text{ and } \lambda_x \simeq 10\lambda_z, \tag{1a}$$

while the latter is self-similar along

$$y \simeq 0.5 \sim 0.7\lambda_z \text{ and } \lambda_x \simeq 2 \sim 3\lambda_z. \tag{1b}$$

This scaling further suggests that the smallest attached eddy with $\lambda_z^+ \simeq 100$ would be a near-wall coherent motion given in the form of a streak and quasi-streamwise vortices aligned to that, whereas the largest one with $\lambda_z \simeq 1.5h$

would be an outer motion with a very-large-scale motion (VLSM) and large-scale motions (LSMs) aligned to that. The attached eddies in-between, the size of which is proportional to their distance from the wall, contribute to the logarithmic region and fill the space caused by the length scale separation. It should be stressed that, to the best of our knowledge, this description incorporates all the coherent structures known in high-Reynolds-number wall-bounded turbulence.

The goal of the present study is to extend our recent work (Hwang, 2015) in order to explore the 'dynamical' self-similarity of the attached eddies. To this end, we will consider the smallest computational domain, which allows each of the attached eddies at the given spanwise length scale to be sustained by themselves, and examine the detailed physical processes that a single attached eddy experiences.

Numerical experiment

The minimal attached eddies

The numerical experiment in the present study is performed in a turbulent channel. We denote x, y, and z as the streamwise, wall-normal, and spanwise directions, respectively. The height of the channel is chosen to be $2h$, and its upper and lower walls are set to be located at $y = 0$ and $y = 2h$, respectively. As in Hwang (2015), the numerical experiment of the present study has been carried out with the static Smagorinsky model, which will be used to damp out the motions smaller than a given spanwise length scale. The residual stress of the static Smagorinsky model is modelled as $\tau_{ij} - \tau_{kk}\delta_{ij}/3 = -2\nu_t\tilde{S}_{ij}$ with $\nu_t = (C_s\tilde{\Delta})^2 D(2\tilde{S}_{ij}\tilde{S}_{ij})^{1/2}$, where $\tilde{\cdot}$ indicates the filtered quantity with the corresponding LES filter, S_{ij} the strain-rate tensor, C_s the Smagorinky, $\tilde{\Delta}$ the filter width of the present LES which uses the grid filter, and $D = 1 - exp[-(y^+/A^+)^3]$ the Van Driest damping function, respectively. We note that the Smagorinsky constant, which generates the best *posterior* performance, has been known to be $C_s = 0.05$ (Härtel & Kleiser, 1998), thus this value will be used for reference simulations.

As in Hwang (2015), self-sustaining attached eddies at a given spanwise length scale are isolated by combining the over-damped LES based on the Smagorinsky model (Hwang & Cossu, 2010*b*) with explicit filtering technique combining with the spanwise narrow computational domain (Hwang, 2013). The over-damped LES, which damps out the motions smaller than the given spanwise length scale $\lambda_{z,0}$, is realised by increasing the Smagorinsky constant C_s to an appropriate value, whereas the explicit filtering technique is implemented by considering the spanwise computational box size $L_z = \lambda_{z,0}$ with removal of the spanwise uniform motions $\widehat{RHS}_u(y; k_x \neq 0, k_z = 0) = 0$ and $\widehat{RHS}_v(y; k_x \neq 0, k_z = 0) = 0$ where $\widehat{RHS}_u$ and $\widehat{RHS}_v$ are respectively the Fourier-transformed streamwise and wall-normal components of the right-hand side of the momentum equation. For further details, the reader may refer to Hwang (2015).

As mentioned, in the present study, we will consider the smallest computational box which allows the given attached eddies to be sustained by themselves (i.e. the minimal unit). The size of such a minimal computational box has been found to be $L_x/L_z = 2.0$ for a given $L_z = \lambda_{z,0}$ (Hwang & Cossu, 2011). In the present study, we will examine the detailed turn-over of a single attached eddy in the corresponding minimal unit with particular emphasis on comparison of the attached eddy in full-scale simulation with $C_s = 0.05$ with that in the filtered simulation with an appropriate value of $C_s > 0.5$ which isolates the attached eddy at the given spanwise length scale. The detailed computational parameter is summarised in table 1.

Case	Re_τ	L_z	$N_x \times N_z$	C_s
$L950a$	941	0.75	$36 \times 81 \times 36$	0.05
$LS950a$	936	0.75	$36 \times 81 \times 36$	0.20
$L950b$	976	1.0	$48 \times 81 \times 48$	0.05
$LS950b$	1004	1.0	$48 \times 81 \times 48$	0.25
$O950$	997	1.5	$72 \times 81 \times 72$	0.05
$OS950$	1152	1.5	$72 \times 81 \times 72$	0.40
$L1800a$	1446	0.375	$36 \times 129 \times 36$	0.05
$LS1800a$	1438	0.375	$36 \times 129 \times 36$	0.20
$L1800b$	1606	0.5	$48 \times 129 \times 48$	0.05
$LS1800b$	1685	0.5	$48 \times 129 \times 48$	0.30
$L1800c$	1745	0.75	$72 \times 129 \times 72$	0.05
$LS1800c$	1954	0.75	$72 \times 129 \times 72$	0.40

Table 1. Simulation parameters. Here, $L_x = 2L_z$ and the resolution is before dealiasing. We note that the first six simulations are performed at $Re_m = 38133$ (Re_m the Reynolds number based on the bulk velocity), while the rest of the simulations are conducted at $Re_m = 73333$.

Results and discussions

The outer attached eddies: VLSM and LSM

We first consider the largest minimal attached eddies scaling in the outer units ($O950$ and $OS950$ in table 1). As shown by Hwang (2015), the spanwise size of the attached eddies of this type is $\lambda_z = 1.5h$, and it consists of a long streaky motions and vortical structures, which are respectively known as VLSM and LSMs. We note that the VLSM is the major carrier of streamwise velocity fluctuations while the LSM is featured to be relatively isotropic in the sense that they carry all the velocity fluctuations. Given this nature, the VLSM would be characterised well with the streamwise velocity fluctuation whereas the LSM would be well featured by the wall-normal or spanwise velocity fluctuations, as also shown by Hwang (2015). We therefore introduce the temporal evolution of the two structures by respectively monitoring the streamwise and wall-normal turbulent kinetic energies, E_u and E_v, obtained by integrating over the lower half of the computational domain: i.e.

$$E_u = 2/V \int_0^{L_x}\int_0^{L_z}\int_0^{L_y/2} (u'/u_\tau)^2 \, dydzdx, \qquad (2a)$$

$$E_v = 2/V \int_0^{L_x}\int_0^{L_z}\int_0^{L_y/2} (v'/u_\tau)^2 \, dydzdx, \qquad (2b)$$

where $V = L_x L_y L_z$.

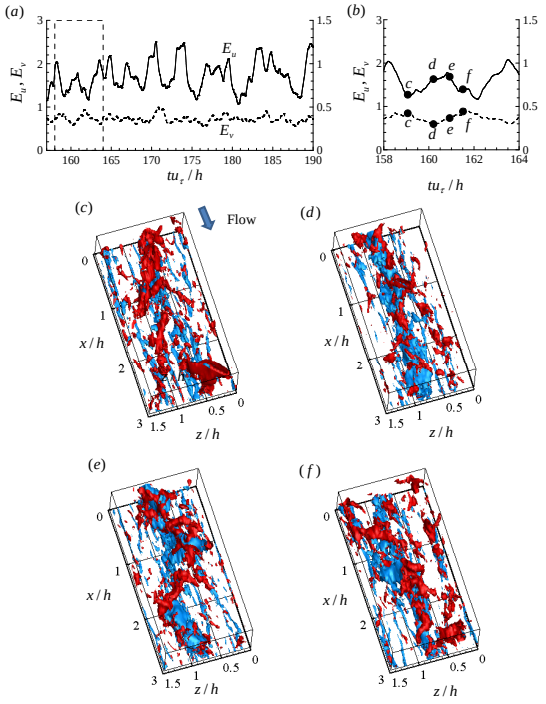

Figure 1. Time evolution of the flow field ($O950$): (a) time trace of the streamwise and wall-normal turbulent kinetic energies E_u (solid) and E_v (dashed); (b) Magnification of (a) for $tu_\tau/h \in [158, 164]$; $(c-f)$ the corresponding flow visualisation at $tu_\tau/h = 159, 160.2, 160.9, 161.5$. In $(c-f)$, the red and blue iso surfaces indicate $u^+ = -3.2$ and $v^+ = 1.4$, respectively.

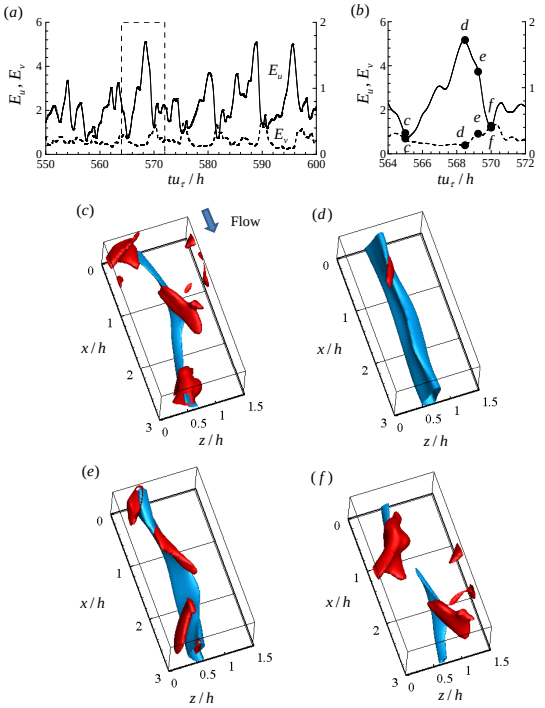

Figure 2. Time evolution of the flow field ($OS950$): (a) time trace of the streamwise and wall-normal turbulent kinetic energies E_u (solid) and E_v (dashed); (b) Magnification of (a) for $tu_\tau/h \in [564, 572]$; $(c-f)$ the corresponding flow visualisation at $tu_\tau/h = 565, 568.5, 569.3, 570$. In $(c-f)$, the red and blue iso surfaces indicate $u^+ = -4$ and $v^+ = 1.5$, respectively.

Fig. 1 shows the temporal evolution of the flow field of $O950$ which also contains the energy-containing motions at $\lambda_z < L_z$. Here, we have to remind the reader that, due to this nature of $O950$, both E_u and E_v, defined in (2), do not strictly monitor the evolution of the outer streaky and vortical structures, although they presumably provide important physical insight into their temporal evolution given their very energetic nature over the entire computational domain. The time trace of E_u and E_v is reported in Fig. 1. Both E_u and E_v exhibit a relatively large-scale intermittent oscillation roughly with the period $Tu_\tau/h = 2 \sim 4$. Furthermore, it appears that the timings of the local maximum of E_u and E_v shows a certain phase difference although it is difficult to assert a certain relationship between E_u and E_v solely with their time trace. For instance, at $tu_\tau/h = 159$, E_v is around the local maximum whereas E_u is at fairly low-energy state (fig 1b). In contrary, at $tu_\tau/h = 160.2$, E_v is roughly at low-energy state whereas E_u becomes considerably large (fig 1b).

The temporal evolution of the flow fields visualised in Figs. 1 $(c-f)$ clearly reveals an interactive dynamics between the structures respectively represented by the streamwise velocity fluctuations. At $tu_\tau/h = 159$ (fig 1c), the flow-field exhibits strong v structures with weak u structures. As the time goes by, the v structures becomes weakened while the u structures are significantly amplified with formation of a large-scale streaky structure, which is clearly the very-large-scale motions in the minimal box. The amplification of the streaky structure carrying intensity energy of the streamwise velocity fluctuation is clearly due to the lift-up effect, which transforms vortical structures carrying the wall-normal velocity fluctuation to streaky structure carrying the streamwise velocity fluctuation by taking energy from the mean shear (del Álamo & Jiménez, 2006; Pujals *et al.*, 2009; Hwang & Cossu, 2010*a*). It is further interesting to note that the amplified streaky structure subsequently experiences strong sinuous bending along the streamwise direction, reminiscent of sinuous instability of amplified streaks (Park *et al.*, 2011). The amplitude of the bent streak becomes gradually weakened and the v structures are significantly amplified again. This process observed here is exactly the same as the bursting in the logarithmic and outer regions described by Flores & Jiménez (2010).

Now, we increase C_s until we remove all the energy-containing structures except at the largest one at $\lambda_z = 1.5h$ (i.e. $OS950$), and inspect temporal evolution of the flow field as shown in Fig. 2. As in $O950$ which contains all the energy-containing motions, the time trace of E_u and E_v oscillates with the time scale of $Tu_\tau/h = 2 \sim 4$ and they show a certain phase difference from each other (figs 2a,b). The flow fields shown in Figs 2$(c-f)$ clearly suggest that qualitatively the same behaviour is observed in the filtered simulation $OS950$: 1) streak amplification via the lift-up effect (from fig 2a to b); 2) sinuous bending via the secondary instability (from fig 2b to c); 3) regeneration of the vortical structure containing the wall-normal velocity

(from fig 2*c* to *d*). It should be stress that this process is very similar to the so-called self-sustaining process described by Hamilton *et al.* (1995), suggesting that the bursting observed both in *O*950 and *OS*950 essentially originates from the self-sustaining dynamics of the outer structures composed of a VLSM and LSMs aligned to that.

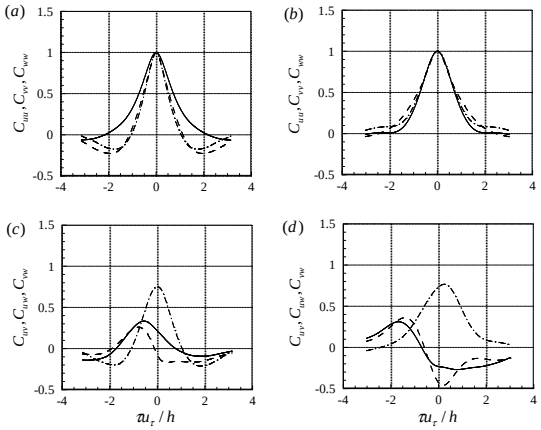

Figure 3. Auto- and cross-correlation functions of (a,c) *O*950 and (b,d) *OS*950 : (a,b) $C_{uu}(\tau)$ (solid), $C_{vv}(\tau)$ (dashed), $C_{ww}(\tau)$ (dashdotted); (c,d) $C_{uv}(\tau)$ (solid), $C_{vw}(\tau)$ (dashed), $C_{uw}(\tau)$ (dashdotted).

To more quantitatively examine the bursting behaviour of the outer structures in the minimal box, we compute auto- and cross-correlation functions in time using the time trace of E_u, E_v and E_w (E_w is defined in the same way with (2)): for example, the cross-correlation function C_{uv} is defined using $E_u(t)$ and $E_v(t)$ such that

$$C_{uv}(\tau) = \frac{\langle E_u(t+\tau)E_v(t)\rangle}{\sqrt{\langle E_u(t)^2\rangle}\sqrt{\langle E_v(t)^2\rangle}}, \qquad (3)$$

where $\langle\cdot\rangle$ denote the time average. All the possible combinations among E_u, E_v and E_w are considered to compute such auto- and cross-correlation functions, which are reported in Fig. 3. We remind that, in the case of *O*950, the energy traces E_u, E_v and E_w are obtained by integrating over the entire computational domain, thereby they do not exactly represent the behaviour of the outer-scaling structures. On the other hand, the energy traces of *OS*950 contains only the outer-scaling structures although their dynamics may also be affected by the non-realistic eddy viscosity. Therefore, Fig. 3 has to be carefully examined, keeping this in mind.

The auto-correlation functions, C_{uu}, C_{vv} and C_{ww}, of both *O*950 (fig 3*a*) and *OS*950 (fig 3*b*) reach or become close to zero at $|\tau u_\tau/h| \simeq 1 \sim 2$, consistent with the bursting period $Tu_\tau/h \simeq 2 \sim 4$. The cross-correlation functions, C_{uv}, C_{uw} and C_{vw}, also show non-trivial behaviours at $|\tau u_\tau/h| < 2$ for both *O*950 and *OS*950. Especially, C_{vw} of both of the simulations shows very strong correlations (i.e. $C_{vw}(\tau = 0) \simeq 0.7 \sim 0.8$), indicating that the v velocity fluctuations visualised in figs 1 and 2 are basically a part of the vortical structure mainly composed of the cross-streamwise velocity components (i.e. streamwise vortices). On the other hand, C_{uv} and C_{uw} of both of the simulations clearly show the phase difference between E_u and E_v (or E_w). Since E_u roughly represents the energy of the streaky structure and both E_v and E_w represent the energy of the streamwise vortical structure, this clearly suggests the presence of the self-sustaining process in *O*950 simulation described by the interactive dynamics between streaks and streamwise vortices observed in *OS*950: i.e. by streak amplification, its breakdown via the sinuous instability, and subsequent regeneration of vortical structures.

Although the correlation functions of *O*950 and *OS*950 are found to behave qualitatively similar, it should also be mentioned that the two simulations exhibit some quantitative differences. We are currently investigating the origin of this difference and have been finding that the difference originate form the small-scale fluctuations in *O*950 as well as from the artificial eddy viscosity in *OS*950. However, the detailed difference will not be discussed in this paper, and will be presented in the near future.

The attached eddies in the logarithmic region

Now, we consider energy-containing motions, the spanwise length scale of which is proportional to the distance from the wall: i.e. $\lambda_z \sim y$. As discussed, the energy-containing motions larger than at a given spanwise length scale at $\lambda_{z,0}$ are removed by setting the spanwise computational domain to be $L_z = \lambda_{z,0}$ with the explicit filtering of the spanwise uniform components, while those smaller than $\lambda_{z,0}$ are damped out by increasing C_s. We start by confirming that the isolated energy-containing motions are the attached eddies.

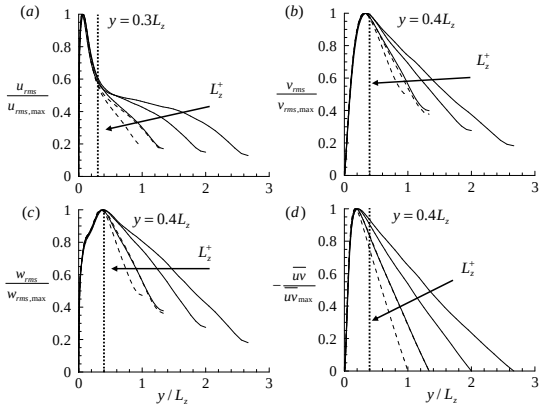

Figure 4. Normalised second-order statistics of the motions rescaled with the given spanwise length L_z: (a) streamwise velocity; (b) wall-normal velocity; (c) spanwise velocity; (d) Reynolds stress. Here, ———, from $Re_\tau \simeq 950$ (*LS*950*a*, *LS*950*b*); - - - -, from $Re_\tau \simeq 1800$ (*LS*1800*a*, *LS*1800*b*, *LS*1800*c*).

Figure 4 shows velocity fluctuations of the isolated motions at a given spanwise length scale. Here, each of the velocity fluctuations is normalised with its peak value, and the wall-normal coordinate is rescaled with the spanwise length scale, $\lambda_{z,0}(= L_z)$ (table 1). As in Hwang (2015), all of the

velocity fluctuations and the Reynolds stress are found to be self-similar with the spanwise length scale L_z for $y \leq 0.3 \sim 0.4L_z$. It is apparent that the self-similar part of the isolated attached eddies exhibit the statistical structure consistent with those hypothesised by Townsend (1976): i.e. the streamwise and the spanwise velocity fluctuations clearly show non-negligible amounts of energy close to the wall ($y < 0.05L_z$ in figures 4*a* and *c*), whereas the wall-normal velocity fluctuation and the Reynolds stress are considerably smaller in that region (figures 4*b* and *d*). The non-self-similarity of the isolated attached eddies for $y \leq 0.3 \sim 0.4L_z$ is simply because the wall-normal locations of the non-self-similar part are supposed to to be 'empty' due to the absence of the motions at $\lambda_z > L_z$. As discussed in Hwang (2015), the non-self-similar part would therefore simply be the fluctuation induced by the self-similar part.

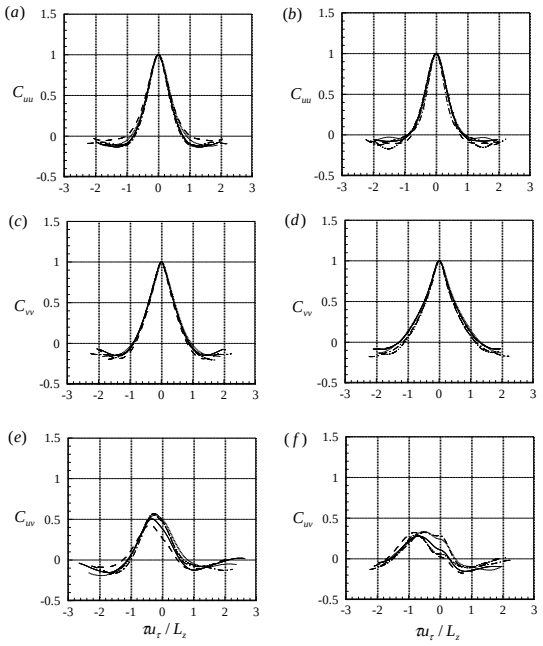

Figure 5. Auto- and cross-correlation functions: (a,b) $C_{uu}(\tau)$; (c,d) $C_{vv}(\tau)$; (e,f) $C_{uv}(\tau)$. In (a,c,e), ——— $L950a$; - - - - $L950b$; —·—·— $L1800a$; —··—··— $L1800b$; ····· $L1800c$, while, in (b,d,f), ——— $LS950a$; - - - - $LS950b$; —·—·— $LS1800a$; —··—··— $LS1800b$; ····· $LS1800c$.

The auto- and cross-correlation functions, C_{uu}, C_{vv}, and C_{uv}, are computed by considering five different attached eddies in the full and the filtered simulations (see table 1). The time scale τ of the computed correlation functions is then rescaled with the spanwise length scale L_z of each of the simulations to examine dynamical self-similarity of the attached eddies. The auto- and cross-correlation functions in the rescaled time coordinate $\tau u_\tau/h$ are shown in Fig. 5. All the correlation functions of both the full and the filtered simulations reasonably well collapse with one another. Especially, the cross-correlation functions ($C_{uv}(\tau)$) of both of the simulation shows the phase difference between E_u and E_v and are found to be qualitatively similar to each other. This strongly suggests that the dynamical self-similarity found here is due to the self-sustaining nature of each of the attached eddies described previously. Furthermore, given that fact that both C_{uu} and C_{vv} reach zero roughly at $|\tau u_\tau/h| = 1$, suggesting that the time scale of the self-sustaining process involving streak amplification, breakdown and regeneration of streamwise vortical structures would be $Tu_\tau/L_z \simeq 2 \sim 4$.

Concluding remarks

So far, we have examined the detailed physical process of the attached eddies by inspecting their temporal evolution using the full and filtered simulations in the minimal computational box for each of the attached eddies. The qualitative similarity between the time correlation functions of the full and the filtered simulations strongly suggest that the attached eddies at all length scale bear a self-sustaining mechanism composed of streak amplification via the 'lift-up' effect, breakdown via its instability, and regeneration of streamwise vortical structures. The time scale of this process, which has also been known as 'bursting', is found to be

$$Tu_\tau/L_z \simeq 2 \sim 3. \tag{4}$$

This time scale compares reasonably well with the one found in Flores & Jiménez (2010), $Tu_\tau/y \simeq 6$, if $y \simeq 0.3 \sim 0.4L_z$ is considered as shown in Fig. 4. This suggests that the bursting found in Flores & Jiménez (2010) is likely due to the self-similar cyclic dynamics caused by the self-sustaining process. Furthermore, if the spanwise length scale is chosen as the spanwise spacing of the near-wall motions (i.e. $L_z^+ \simeq 100$), the well-known time scale of near-wall bursting is obtained ($T \simeq 200 \sim 300\nu/u_\tau^2$) Jiménez & Moin (1991). On the other hand, if the spanwise spacing of the large-scale and the very-large-scale motions is chosen (i.e. $L_z \simeq 1.5h$), it well retrieves $Tu_\tau/h \simeq 3 \sim 4.5$. This self-similarity of the dynamics complements our recent work (Hwang, 2015) which established the self-similarity of statistical structure of the attached eddies.

REFERENCES

del Álamo, J. C. & Jiménez, J. 2006 Linear energy amplification in turbulent channels. *J. Fluid Mech.* **559**, 205–213.

Flores, O. & Jiménez, J 2010 Hierarchy of minimal flow units in the logarithmic layer. *Phys. Fluids* **22**, 071704.

Hamilton, J.M., Kim, J. & Waleffe, F. 1995 Regeneration mechanisms of near-wall turbulence structures. *J. Fluid Mech* **287**, 317–348.

Härtel, C. & Kleiser, L. 1998 Analysis and modelling of subgrid-scale motions in near-wall turbulence. *J. Fluid Mech* **356**, 327–352.

Hwang, Y. 2013 Near-wall turbulent fluctuations in the absence of wide outer motions. *J. Fluid Mech.* **723**, 264–288.

Hwang, Y. 2015 Statistical structure of self-sustaining attached eddies in turbulent channel flow. *J. Fluid Mech.* **767**, 254–289.

Hwang, Y. & Cossu, C. 2010*a* Linear non-normal energy

amplification of harmonic and stochastic forcing in the turbulent channel flow. *J. Fluid Mech.* **664**, 51–73.

Hwang, Y. & Cossu, C. 2010*b* Self-sustained process at large scales in turbulent channel flow. *Phys. Rev. Lett.* **105**, 044505.

Hwang, Y. & Cossu, C. 2011 Self-sustained processes in the logarithmic layer of turbulent channel flows. *Phys. Fluid* **23**, 061702.

Jiménez, J. & Hoyas, S. 2008 Turbulent fluctuations above the buffer layer of wall-bounded flows. *J. Fluid Mech.* **611**, 215–236.

Jiménez, J. & Moin, P. 1991 The minimal flow unit in near-wall turbulence. *J. Fluid Mech.* **225**, 213–240.

Marusic, I., Monty, J. P., Hultmark, M. & Smits, A. J. 2013 On the logarithmic region in wall turbulence. *J. Fluid Mech.* **716**, R3.

Park, J., Hwang, Y. & Cossu, C. 2011 On the stability of large-scale streaks in the turbulent Couette and Poiseulle flows. *C. R. Mècanique* **339** (1), 1–5.

Perry, A. E. & Chong, M. S. 1982 On the mechanism of turbulence. *J. Fluid Mech.* **119**, 173–217.

Pujals, G., García-Villalba, M., Cossu, C. & Depardon, S. 2009 A note on optimal transient growth in turbulent channel flows. *Phys. Fluids* **21**, 015109.

Townsend, A. A. 1976 *The structure of turbulent shear flow*. Cambridge U. Press.